



HAL
open science

Departure from centrosymmetry of red giants and supergiants measured with VLTI/AMBER

P. Cruzalèbes, A. Jorissen, A. Chiavassa, C. Paladini, Y. Rabbia, Alain Spang

► **To cite this version:**

P. Cruzalèbes, A. Jorissen, A. Chiavassa, C. Paladini, Y. Rabbia, et al.. Departure from centrosymmetry of red giants and supergiants measured with VLTI/AMBER . Monthly Notices of the Royal Astronomical Society, 2015, 446 (4), pp.3277-3284. 10.1093/mnras/stu2382 . hal-03526447

HAL Id: hal-03526447

<https://hal.science/hal-03526447>

Submitted on 15 Jan 2022

HAL is a multi-disciplinary open access archive for the deposit and dissemination of scientific research documents, whether they are published or not. The documents may come from teaching and research institutions in France or abroad, or from public or private research centers.

L'archive ouverte pluridisciplinaire **HAL**, est destinée au dépôt et à la diffusion de documents scientifiques de niveau recherche, publiés ou non, émanant des établissements d'enseignement et de recherche français ou étrangers, des laboratoires publics ou privés.



Distributed under a Creative Commons Attribution 4.0 International License

Departure from centrosymmetry of red giants and supergiants measured with VLT/AMBER[★]

P. Cruzalèbes,^{1†} A. Jorissen,² A. Chiavassa,¹ C. Paladini,² Y. Rabbia¹ and A. Spang¹

¹Laboratoire Lagrange, UMR 7293, Université de Nice-Sophia Antipolis, CNRS, Observatoire de la Côte d’Azur, Bd de l’Observatoire, CS 34229, F-06304 Nice cedex 4, France

²Institut d’Astronomie et d’Astrophysique, Université Libre de Bruxelles, Campus Plaine C.P. 226, Bd du Triomphe, B-1050 Bruxelles, Belgium

Accepted 2014 November 7. Received 2014 November 7; in original form 2014 October 3

ABSTRACT

We study a sample of 16 bright and well-resolved late-type stars (10 O-rich giants, 2 red supergiants, and 4 C-rich giants) using the ESO VLT/AMBER facility at medium resolution ($\mathcal{R} = 1500$) in the K band to detect and measure the deviation from centrosymmetry of their resolved surface brightness distribution. As indicator for departure from centrosymmetry, we use the centrosymmetry parameter (CSP). We observe that CSP increases along the asymptotic giant branch, reaching values as large as 30° . These large CSP values are likely attributable to a few large photospheric convective cells. Carbon stars like W Ori and R Scl, being close to the AGB tip, have the second largest CSP values (17.6 and 22.3 , respectively), being only surpassed by the M5.5Ib/II supergiant T Cet (with CSP of 30.4). For K and early M giants, CSP values are smaller, never exceeding 10° , with a clear tendency to increase with the atmospheric pressure scaleheight. This supports the hypothesis that the observed deviations from centrosymmetry are somehow related to convective cells, whose size depends upon the atmospheric pressure scaleheight.

Key words: methods: data analysis – techniques: interferometric – stars: atmospheres – stars: fundamental parameters – stars: late-type.

1 INTRODUCTION

Many high-angular resolution observations of evolved stars have shown departure from centrosymmetry of their photospheres (e.g. Wilson et al. 1992; Tuthill, Haniff & Baldwin 1997, 1999; Hofmann et al. 2000; Thompson, Creech-Eakman & Akeson 2002; Ragland et al. 2006; Weiner et al. 2006; Woodruff et al. 2008; Kervella et al. 2009; Ohnaka et al. 2009, 2011; Wittkowski et al. 2011, 2012; Paladini et al. 2012; van Belle et al. 2013). Three-dimensional (3D) radiation hydrodynamics (RHD) simulations carried out with the CO5BOLD¹ code (Freytag et al. 2012) for asymptotic giant branch stars (AGBs; Freytag & Höfner 2008) and red supergiants (RSGs; Chiavassa et al. 2011b) reveal that large convective cells produce patterns at the apparent stellar surface (more noticeable in the infrared than in the visible) with a typical size comparable to the stellar radius, and evolving on a time-scale of years. On top of these

cells, small convective structures (most conspicuous in the visible), with a size of about 5–10 percent of the stellar radius, evolve on time-scales of weeks to months. The latter features result from the opacity variation and the gas dynamics at optical depths smaller than unity, i.e. farther up in the atmosphere with respect to the continuum-forming region (Chiavassa et al. 2011a). In Chiavassa et al. (2009), different reasons were pointed out for the peculiar convective pattern: (i) in RSGs, most of the downdrafts will not grow fast enough to reach any significant depth before they are swept into the existing deep and strong downdrafts enhancing the strength of neighbouring downdrafts; (ii) radiative effects and smoothing of small fluctuations could matter; (iii) sphericity effects and/or numerical resolution (or lack of it).

Thus, the large photospheric convective cells predicted by these 3D RHD simulations must generate surface brightness asymmetries (SBAs), which are responsible for the observed deviations from centrosymmetry. For less-evolved K and M giants, 3D RHD simulations predict a convective granulation made out of smaller cells, whose size is related to the atmospheric pressure scaleheight (Freytag 2001; Svensson & Ludwig 2005).

The goal of the present study is to go a step further in the investigation of the properties of stellar surface convection. We track the onset and properties of the deviation from centrosymmetry, in connection with the location of the star in the Hertzsprung–Russell

[★]Based on observations made with ESO telescopes at the Paranal Observatory under Belgian VISA Guaranteed Time programme ID 083.D-029(A/B), 084.D-0131(A/B), 086.D-0067(A/B/C).

[†]E-mail: pierre.cruzalebes@oca.eu

¹Acronym of *CO*nservative *CO*de for the *CO*mputation of *CO*mpressible *CO*nvection in a *BO*x of *L* Dimensions with $l = 2, 3$.

diagram (HRD; Section 3). Since the 3D RHD simulations predict a strong sensitivity of SBAs to the atmospheric pressure scaleheight, which controls the size of the convective cells, we search for a possible connection between deviation from centrosymmetry and atmospheric pressure scaleheight in Section 4. Finally, we find that supergiants and C-rich AGB stars have the largest CSP values.

To achieve our research goals, we acquired VLTI/AMBER measurements in the medium-resolution *K* band (MR-*K*) for a sample of 16 well-resolved late-type stars scattered across the upper right of the HRD (10 O-rich giants, 2 RSGs, and 4 C-rich giants; Section 2).

If not based on direct imaging, the detection of SBAs usually relies on the so-called triple product, involving complex visibilities from interferometric observations using simultaneously three apertures. To characterize the asymmetry of the source morphology with a single indicator, we use the centrosymmetry parameter (CSP) based on a sum, spanning the observation spectral band, of absolute values of the imaginary part of the triple product (Cruzalèbes et al. 2013a, 2014). With such a definition, a null CSP can only occur if the triple product is identically null all over the spectral band considered, i.e. if there is no deviation from centrosymmetry at any wavelength.² We refer the reader to our previous paper in this series (Cruzalèbes et al. 2014) for a detailed study about how CSP behaves under specific circumstances, like a stellar surface covered by a few convective spots, a tidally deformed (pear-shaped) stellar disc or a resolved binary star. This former study concludes that the CSP parameter has no power to specifically distinguish between these various models, but is excellent at raising the flag of SBAs.

The use of an indicator like CSP will be an essential tool in future searches for asymmetries using archive data for sample of objects observed with limited *uv*-coverage, thus allowing no reliable image reconstruction. We think that CSP could be also used to identify asymmetric targets when dealing with snapshot surveys.

Finally, it should be stressed that this paper only presents a global analysis of the collected material. Discussion on individual targets will be submitted as separate forthcoming papers.

The results and graphical outputs presented in the paper have been obtained using the modular software suite SPIDAST,³ created to calibrate spectro-interferometric measurements and to interpret them by using chromatic models (Cruzalèbes, Spang & Sacuto 2008; Cruzalèbes et al. 2010, 2013a).

Throughout this paper, uncertainties are reported using the concise notation, according to the recommendation of the Joint Committee for Guides in Metrology (JCGM-WG1 2008). The number between parentheses is the numerical value of the standard uncertainty referred to the associated last digits of the quoted result. For instance, a value denoted ‘38.6(36)’ means ‘38.6 ± 3.6’. In the same way, a value denoted ‘38.60(36)’ means ‘38.60 ± 0.36’.

2 INTRODUCING THE OBSERVATIONS

2.1 Selecting the science targets for the programme

The sample contains red giants, supergiants, and long-period variables, bright enough ($m_K < 2$) to be measured by the VLTI subarray (1.80 m auxiliary telescopes) with high signal-to-noise ratio (SNR).

² We leave aside the obvious situation where the star is too far away for the stellar surface to be resolved by the interferometer so that it appears as point like, giving naturally a null CSP what prevents to detect any deviation from centrosymmetry.

³ Acronym of *SP*ectro-*I*nterferometric *D*ata *A*nalysis *S*oftware *T*ool.

On one hand, the scientific targets must be resolved well enough, which results in visibilities clearly smaller than unity. On the other hand, too small visibilities prevent the fringe-tracking system from working under optimal conditions, producing poor-quality data sets (caused by ill-stabilized fringes). Applying these two contradictory constraints to the AMBER instrument operating in the *K* band, with baseline lengths up to 100 m, leads to choose resolved scientific targets with approximately the same expected angular diameter of 10 mas (i.e. about twice the angular resolution of the interferometer). Under such circumstances, our targets should be easily resolved by the interferometer, so that any deviation from centrosymmetry should be revealed by a non-zero value of the CSP parameter (see footnote 2).

2.2 Observation logbook

16 cool stars (10 O-rich giants, 2 RSGs, and 4 C-rich giants) were observed in 2009 May (three nights), 2009 August (two nights), 2009 November (three nights), 2010 March (three nights), and 2010 December (four nights), using the AMBER instrument at the focus of the ESO/VLTI, with three auxiliary telescopes. All observations (their logbook is provided in Table 1) were done using the MR-*K* spectral configuration (about 500 spectral channels with $\mathcal{R} = 1500$) centred at $\lambda = 2.3 \mu\text{m}$. All details regarding data reduction and calibration (using the SPIDAST software) can be found in Cruzalèbes et al. (2013a). The angular diameters of the targets have been derived in Cruzalèbes et al. (2013b) by using centre-to-limb profiles from MARCS (Gustafsson et al. 2008) and TURBOSPECTRUM (Alvarez & Plez 1998; Plez 2012) to fit the visibility measurements. For the sake of completeness, these angular diameters are repeated in Table 2.

Since the goal of our study is to discriminate between centrosymmetric and non-centrosymmetric brightness distributions, in our observation strategy we have gathered measurements obtained with different baseline orientations, so as to be sensitive to the azimuthal variation of the brightness distribution (see Fig. 1).

2.3 Definition of CSP

The CSP parameter used to characterize the deviation from centrosymmetry has been introduced in Cruzalèbes et al. (2013a) and studied in detail in Cruzalèbes et al. (2014). It is defined as

$$\sin(\text{CSP}) = \frac{\int_{\lambda_1}^{\lambda_2} |\Im \mathcal{T}_{123}(\lambda)| d\lambda}{\int_{\lambda_1}^{\lambda_2} |\Re \mathcal{T}_{123}(\lambda)| d\lambda}, \quad (1)$$

where \mathcal{T}_{123} is the triple product measured for a given baseline triplet. We recall that a small CSP value corresponds to a centrosymmetric brightness distribution, and that, conversely, a CSP value clearly departing from zero degree (taking into account the uncertainty) indicates a brightness distribution deviating from centrosymmetry. Moreover, using numerical simulations with a simple spot model, we showed (in section 2.4 of Cruzalèbes et al. 2014) that for a given geometric configuration of the spot, CSP is not very sensitive to the photometric contrast between the spot and the stellar disc (at least for interferometric observations not probing beyond the second lobe).

Fig. 2 shows the spectral distributions of the real and imaginary parts of \mathcal{T}_{123} , for seven individual observing blocks (OBs) associated with various scientific targets. The ‘spectral mean’ quoted above each panel corresponds to the spectral average of the displayed quantity over the whole spectral band. For the panels at left, it thus equals $\sin(\text{CSP})$. Several stars exhibit sharp and deep

Table 1. Logbook of the observations. Column 2: Modified Julian Date of the observation (MJD = JD-2 400 000.5); column 3: number of OBs; column 4: calibrator used; column 5: VLTI subarray configuration; column 6: mean seeing angle (in arcsecond).

Name	MJD	NOB	Calib.	Config.	ε_0
α Car	55142.2	2	η Col	D0H0K0	2.2
	55143.4	2	η Col	D0H0K0	0.8
	55144.3	1	η Col	D0H0K0	1.2
	55268.1	1	η Col	D0H0K0	1.2
	55270.1	2	η Col	H0K0G1	0.9
β Cet	55539.1	1	η Cet	D0I1G1	0.7
	55540.1	1	η Cet	D0I1H0	0.8
	55542.1	1	η Cet	K0I1G1	1.1
	55543.1	2	η Cet	K0I1A0	1.2
α TrA	54975.3	2	ε TrA	H0D0A0	0.6
	54976.1	2	ε TrA	H0D0A0	0.8
	54977.2	1	ε TrA	H0D0A0	0.8
	55051.1	1	o Sgr	H0D0A0	1.1
	55053.1	2	ε TrA	H0D0A0	1.1
	55268.3	3	ε TrA	D0H0K0	2.4
	55269.3	1	ε TrA	D0H0K0	1.8
	55270.3	3	ε TrA	H0K0G1	0.5
	α Hya	55268.2	3	λ Hya	D0H0K0
55270.3		2	λ Hya	H0K0G1	0.7
ζ Ara	54975.4	1	ε TrA	H0D0A0	0.6
	54976.1	2	ε TrA	H0D0A0	0.9
	54977.1	2	ε TrA	H0D0A0	0.7
	55053.2	2	ε TrA	H0D0A0	1.2
δ Oph	54975.2	2	γ Lib	H0D0A0	0.6
	54976.2	1	γ Lib	H0D0A0	0.7
	54977.2	1	γ Lib	H0D0A0	0.8
	55051.0	3	γ Lib	H0D0A0	0.8
	55053.0	1	γ Lib	H0D0A0	1.6
	55269.4	2	γ Lib	D0H0K0	1.9
	55270.4	1	γ Lib	H0K0G1	0.7
γ Hyi	55539.3	1	α Ret	D0H0I1	0.5
	55540.3	1	α Ret	D0G1I1	0.5
o_1 Ori	55144.2	1	HR 2411	D0H0K0	1.1
σ Lib	55268.4	1	51 Hya	D0H0K0	3.1
	55269.2	1	51 Hya	D0H0K0	1.3
γ Ret	55539.3	2	α Ret	D0H0I1	0.9
	55540.3	3	α Ret	D0G1I1	0.6
CE Tau	55143.3	3	φ_2 Ori	D0H0K0	0.8
	55539.1	6	φ_2 Ori	D0I1G1	0.7
	55540.1	2	φ_2 Ori	D0I1H0	0.8
	55540.2	4	φ_2 Ori	D0I1G1	0.8
	55542.3	2	φ_2 Ori	G1I1A0	1.7
	55543.2	1	φ_2 Ori	K0I1A0	0.7
	55543.2	1	φ_2 Ori	G1I1A0	0.6
	55543.3	1	φ_2 Ori	K0I1G1	0.9
	55543.3	1	φ_2 Ori	K0I1A0	1.5
55543.3	1	φ_2 Ori	G1I1A0	1.5	
T Cet	55142.1	2	γ Scl	D0H0K0	1.5
	55142.2	1	ι Eri	D0H0K0	2.3
	55143.1	1	γ Scl	D0H0K0	0.7
	55144.0	3	γ Scl	D0H0K0	0.8
TX Psc	55142.0	2	θ Psc	D0H0K0	1.1
	55143.1	2	θ Psc	D0H0K0	0.8

Table 1. – continued

Name	MJD	NOB	Calib.	Config.	ε_0
W Ori	55144.1	2	θ Psc	D0H0K0	0.9
	55539.0	2	θ Psc	D0I1G1	0.7
	55540.0	1	θ Psc	D0I1H0	0.9
	55540.1	1	θ Psc	H0I1G1	1.0
	55542.1	1	θ Psc	K0I1G1	1.2
	55543.0	1	θ Psc	K0I1G1	1.4
	55543.1	1	θ Psc	K0I1A0	1.3
	55143.2	3	φ_2 Ori	D0H0K0	0.7
	55144.2	1	φ_2 Ori	D0H0K0	0.8
	55270.1	1	HR 2113	H0K0G1	0.6
R Scl	55143.0	4	ι Eri	D0H0K0	0.7
	55144.1	1	ι Eri	D0H0K0	0.6
TW Oph	54975.4	2	o Sgr	H0D0A0	0.8
	54976.2	1	γ Lib	H0D0A0	0.7
	54977.2	2	γ Lib	H0D0A0	0.8
	54977.3	1	o Sgr	H0D0A0	0.8
	55051.2	1	o Sgr	H0D0A0	1.1
	55053.2	1	o Sgr	H0D0A0	1.1

Table 2. Mean CSP (last column, in degree), obtained by weighted averages over the OBs. The third column labelled ϕ gives the angular diameter (in milliarcsecond) from Cruzalèbes et al. (2013b).

Name	Sp. type	ϕ	CSP
α Car	F0II	6.92(11)	1.1(5)
β Cet	K0III	5.51(25)	1.3(3)
α TrA	K2II	9.24(2)	2.5(6)
α Hya	K3II-III	9.36(6)	2.2(9)
ζ Ara	K3III	7.09(12)	1.4(2)
δ Oph	M0.5III	9.93(9)	1.3(5)
γ Hyi	M2III	8.79(9)	3.7(12)
o_1 Ori	M3III	9.78(10)	8.1(8)
σ Lib	M3.5III	11.33(10)	5.1(2)
γ Ret	M4III	7.44(2)	9.1(16)
CE Tau	M2Iab-b	9.97(8)	5.3(9)
T Cet	M5.5Ib/II	9.70(8)	30.4(17)
TX Psc	C7.2	10.23(36)	11.2(35)
W Ori	C5.4	9.63(4)	17.6(45)
R Scl	C6,5sea	10.06(5)	22.3(67)
TW Oph	C5.5	9.46(30)	3.1(5)

variations beyond 2.3 μm (likely to trace the effects of the CO spectral bands). One may wonder what impact these spectral features have on the final CSP value. To answer that question, we selected the star T Cet for which the CO bands are the strongest. The CSP for T Cet from the specific OB displayed in Fig. 2 amounts to $28^\circ \pm 1^\circ$ with the integration (equation 1) spanning the whole spectral band (thus including the CO bands), as compared to $30^\circ \pm 1^\circ$ when the integration does not go beyond 2.3 μm (thus excluding the CO bands). The effect is thus small (even for this extreme case), and this could be expected since CSP is an integrated property, thus smoothing away local variations like those linked to the CO bands. On a more physical standpoint, it is nevertheless interesting to realize that the CO bands manifest themselves in the triple product, in the sense of reducing the deviations from centrosymmetry. This is especially noteworthy for R Scl, where the imaginary part of the triple product

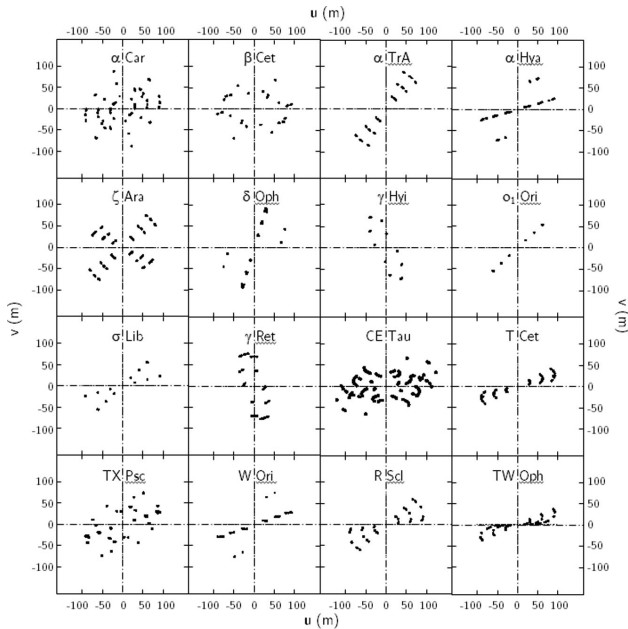


Figure 1. Global (u, v) coverage obtained with all observations, for each scientific target.

stays close to zero in the whole spectral region covered with CO bands.

The final set of CSP values is given in the last column of Table 2. They are computed by using the weighted sum over the OBs, with weights given by the squared inverse of the individual uncertainties. The final uncertainty is derived from the variance of the bootstrapped distribution of the weighted means, obtained by random sampling with replacement of the individual CSP values with their associated uncertainties (direct-bootstrap method; Efron & Tibshirani 1993). In case of a too small number of available OBs, the bootstrap method cannot be used, and the final uncertainty is given by the standard deviation of the weighted mean, as given by Galassi et al. (2009).

Using the same criterion as the one used by Ragland et al. (2006), based on the closure phase in the H band as indicator for asymmetry, we consider as meaningful a final CSP value greater than twice its uncertainty ($\text{SNR} > 2$). Thus, we note that all targets of our sample present various levels of departure (though all being significant): marginal departure ($\text{CSP} < 5^\circ$) for α Car, β Cet, α TrA, α Hya, ζ Ara, δ Oph, γ Hvi, and TW Oph; moderate suspicion ($5^\circ < \text{CSP} < 10^\circ$) for o_1 Ori, σ Lib, γ Ret, and CE Tau; and clear departure ($\text{CSP} > 10^\circ$) for T Cet, TX Psc, W Ori, and R Scl.

3 HERTZSPRUNG–RUSSELL DIAGRAM (HRD)

In this section, we use the values of the fundamental parameters of our science targets reported in Table 3, to confront their final CSP values with their location in the HRD.

Fig. 3 shows the resulting temperature–luminosity diagrams, for the targets included in our sample. The left-hand panel shows the error bars for the science targets (named, drawn in blue), and for the calibrators (unnamed, green crosses). In order to prevent vertical bars to overlap and to degrade the information, the location of R Scl, W Ori, and TW Oph have been slightly shifted horizontally, although these three carbon stars have the same effective temperature of 2600 K. The right-hand panel shows the CSP values for the science targets as (blue) squares. Their size increases proportionally

to log (CSP) (not proportionally to CSP, for graphical convenience): the stars with brightness distributions far from centrosymmetry are associated with large squares. These two HRDs also display evolutionary tracks from the Padova set (Bertelli et al. 2008, 2009), for $Y=0.26$ and $Z=0.017$, and for masses between 1 and $8 M_\odot$ (Y is the helium abundance, and Z the metallicity).

The right-hand panel of Fig. 3 shows that the stars with the largest asymmetries, i.e. with high final CSP values, are located in the upper-right corner of the HRD. This region is occupied by the stars with the largest radii and Fig. 4 shows a tendency for CSP to increase with \mathcal{R} (the Rosseland radius reported in Table 3). Although a number of relations could go through the points in the $\log \mathcal{R}$ – \log (CSP) diagram, a linear fit is shown to fix the ideas, not assuming any physical relevance.

To anticipate the reader’s preference, the same data set is presented in a slightly different way in Fig. 5, displaying the temperature–gravity diagram (using the values of Table 3), with the sizes of the (blue) squares still proportional to log (CSP). This diagram shows more clearly than in the HRD that the value of CSP increases with decreasing T_{eff} and $\log g$: cool supergiants exhibit a higher degree of asymmetry than hotter giants. It also exhibits two groups of targets which can be easily separated according to their temperature and surface gravity:

(I) Stars with hot ($T_{\text{eff}} \gtrsim 4000$ K) and compact ($\log g \gtrsim 1$) atmospheres (included in the bottom-left box of Fig. 5). This group contains all our calibrators, as well as the first five science targets of Table 2. These latter exhibit small CSP values (≤ 2.5).

(II) Stars with cool ($T_{\text{eff}} \lesssim 4000$ K) and diluted ($\log g \lesssim 1$) atmospheres (included in the upper-right box). This group contains the other science targets. Except for δ Oph ($T_{\text{eff}} = 3650 \pm 50$ K, with $\log g = 0.93 \pm 0.12$, very close to unity, taking into account the error bar), they exhibit somewhat large CSP values (≥ 3.7).

The transition between the two groups of stars occurs around $\log g \sim 1$, and as a matter of fact, this value corresponds to a transition encountered as well in the 3D RHD simulations of Chiavassa et al. (2011a). In the RSG/AGB configuration ($\log g < 1$), only a few large convective cells cover the stellar disc, whereas in the giant-star configuration ($\log g > 1$), the stellar disc is covered by a large number of small convective cells.

Schwarzschild (1975) argued that the atmospheric pressure scale-height \mathcal{H}_p drives the characteristic scale of convection. At least for red giants with $2 \leq \log g \leq 4$ and $4000 \leq T_{\text{eff}}(\text{K}) \leq 6000$, this prediction has been confirmed from the observations of ~ 1000 such stars by the Kepler Observatory (Mathur et al. 2011), with the conclusion that the typical size of the convective cells is proportional to \mathcal{H}_p . In the next section, we study therefore the possible correlation between CSP and \mathcal{H}_p .

4 DEVIATION FROM CENTROSYMMETRY AND PRESSURE SCALEHEIGHT

3D RHD simulations predict that the photosphere of red giants and supergiants are covered by convective cells (Chiavassa et al. 2010). Freytag (2001) found that the size of these cells is related to \mathcal{H}_p , defined as

$$\mathcal{H}_p \sim \frac{T_{\text{eff}}}{g}, \quad (2)$$

according to the simplified definition adopted by Chiavassa et al. (2010). The last column of Table 3 gives the values of \mathcal{H}_p

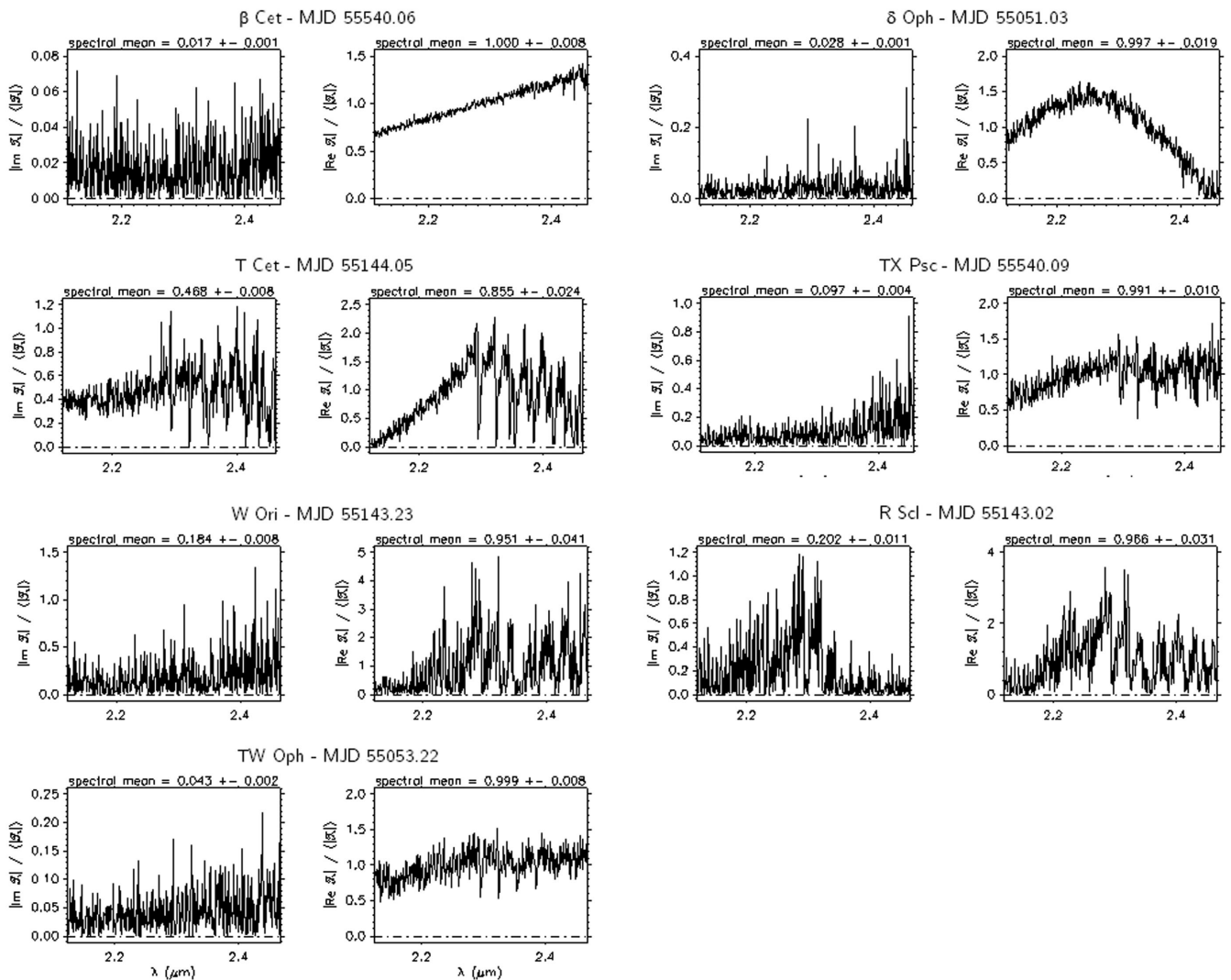


Figure 2. Spectral variation of the complex triple product, for seven different OBs obtained with seven science targets. Left-hand panels: absolute value of the imaginary part of the triple product, divided by the spectral average of the modulus. Right-hand panels: absolute value of the real part of the triple product, divided by the spectral average of the modulus.

derived from the fundamental parameters taken from Cruzalèbes et al. (2013b).

Since the convective cells induce surface inhomogeneities, and thus contribute to the global deviation from centrosymmetry, we study the possible correlation between CSP and \mathcal{H}_P . Fig. 6 shows CSP with respect to \mathcal{H}_P : left-hand panel, for the five science targets with hot and compact atmospheres (group I); right-hand panel, for the 11 science targets with cool and diluted atmospheres (group II). The transition between the two groups of stars occurs for $\log \mathcal{H}_P \sim 2.5$ – 2.6 , in agreement with the transition value $\log \mathcal{H}_P = 2.57$ found for the transition from the giant star models to the RSG/AGB models (fig. 17 of Chiavassa et al. 2011a). In their study of the convective-cell pattern on the surface of RSGs, these authors have investigated the relation between \mathcal{H}_P and the photocentre motion due to the temporal evolution of the convective pattern (denoted σP in their paper).

Here, we follow a similar approach, but using CSP instead of the photocentre motion. Since the two quantities bear some physical relationship with convection, we use the same analytical forms as the ones used by Chiavassa et al. (2011a) between $\log \sigma P$ and $\log \mathcal{H}_P$,

namely a linear relation for stars of group I, and an exponential law for stars of group II (with parameters deduced from least-squares fitting). These relations, along with their analytical expressions, are given in the caption of Fig. 6.

For stars of group I, we find an acceptable linear relationship, albeit with a very small slope, indicating that the link between CSP and \mathcal{H}_P is weak for these stars. For stars of group II, different functional relationships could be used. We chose an exponential as Chiavassa et al. (2011a) arbitrary did for stars of group II, in the aim to fit the transition region between the giant star and the RSG/AGB star model points in the $\log \mathcal{H}_P$ – $\log \sigma P$ diagram, given by the 3D RHD simulation. In any case, Fig. 6 reveals that targets (group II) with their surface covered by a small number of large cells present higher departure from centrosymmetry (hence larger final CSP values) than targets (group I) with many more smaller cells.

For the sake of comparison of group II targets with theory, the final CSP values for two 3D RHD simulations computed with the `co5BOLD` code (Freytag & Höfner 2008; Chiavassa et al. 2011b) are added to the right-hand panel of Fig. 6. The first simulation

Table 3. Fundamental parameters of the science targets (first part from top), of the calibrators (second part), from Cruzalèbes et al. (2013b). The bottom part gives the fundamental parameters of the two 3D RHD simulations used in this paper: from Chiavassa et al. (2009) for the RSG/AGB model; from Freytag & Höfner (2008) for the AGB model.

Name	\mathcal{R}^a	$\log T_{\text{eff}}^b$	$\log \mathcal{L}^c$	M_{bol}^d	\mathcal{M}^e	$\log g^f$	$\log \mathcal{H}_p^g$
α Car	71(4)	3.845(6)	4.03(5)	-5.34(13)	8.0(3)	1.64(5)	2.20(5)
β Cet	17.5(9)	3.668(9)	2.21(6)	-0.54(14)	3.0(3)	2.43(6)	1.24(6)
α TrA	119(2)	3.638(10)	3.66(4)	-4.41(11)	7.5(5)	1.16(3)	2.48(3)
α Hya	55.7(7)	3.633(10)	2.98(4)	-2.71(10)	4.5(5)	1.60(5)	2.04(5)
ζ Ara	114(4)	3.628(10)	3.58(5)	-4.21(12)	7.5(5)	1.20(4)	2.43(4)
δ Oph	56.0(7)	3.562(12)	2.70(5)	-2.01(12)	1.0(3)	0.93(12)	2.64(12)
γ Hya	62.0(8)	3.544(12)	2.71(5)	-2.05(13)	1.0(3)	0.84(12)	2.71(12)
α_1 Ori	214(29)	3.538(13)	3.76(13)	-4.65(31)	3.5(5)	0.32(13)	3.21(13)
σ Lib	108(3)	3.538(13)	3.17(5)	-3.18(14)	1.8(3)	0.61(7)	2.93(7)
γ Ret	115(2)	3.538(13)	3.23(5)	-3.33(13)	1.8(3)	0.55(6)	2.99(6)
CE Tau	601(83)	3.531(13)	4.63(13)	-6.83(32)	8.0(3)	-0.21(12)	3.74(12)
T Cet	286(34)	3.512(13)	3.91(12)	-5.03(30)	3.0(3)	0.01(11)	3.51(12)
TX Psc	322(74)	3.477(14)	3.90($\frac{21}{31}$)	-5.02(61)	1.8(3)	-0.30(21)	3.78(21)
W Ori	406(185)	3.415(17)	3.83($\frac{51}{37}$)	-4.85(103)	1.5(5)	-0.60($\frac{42}{63}$)	4.02(53)
R Scl	513(721)	3.415(17)	4.04($\frac{117}{55}$)	-5.35(201)	2.5(5)	-0.59(75)	4.01(75)
TW Oph	278(102)	3.415(17)	3.50($\frac{42}{34}$)	-4.02(89)	1.0(3)	-0.46($\frac{38}{47}$)	3.88(42)
α Ret	13.5(3)	3.679(9)	1.93(4)	-0.10(11)	2.8(3)	2.61(5)	1.07(5)
φ_2 Ori	8.8(1)	3.669(9)	1.52(4)	0.95(10)	1.5(5)	2.73($\frac{13}{19}$)	0.94(16)
η Col	37.1(13)	3.668(9)	2.77(5)	-2.17(12)	5.0(3)	2.00(4)	1.67(4)
λ Hya	9.7(8)	3.668(9)	1.60(8)	0.74(20)	1.5(5)	2.64($\frac{20}{25}$)	1.03(22)
γ Lib	12.4(6)	3.668(9)	1.81(6)	0.21(14)	2.0(3)	2.55(7)	1.12(7)
σ Sgr	11.7(9)	3.668(9)	1.76(7)	0.33(19)	2.0(3)	2.60(8)	1.07(8)
ι Eri	11.7(10)	3.663(9)	1.74(8)	0.40(21)	1.5(5)	2.48($\frac{20}{25}$)	1.18(23)
θ Psc	10.4(7)	3.662(9)	1.63(7)	0.67(17)	1.3(3)	2.50(14)	1.17(14)
γ Scl	12.3(1)	3.654(10)	1.75(4)	0.37(10)	1.3(3)	2.35(10)	1.31(10)
HR 2113	35(4)	3.647(10)	2.62(10)	-1.82(24)	3.5(5)	1.90(11)	1.75(11)
ε TrA	16.2(2)	3.647(10)	1.96(4)	-0.16(10)	1.5(5)	2.20($\frac{14}{19}$)	1.45(16)
η Cet	13.6(1)	3.647(10)	1.81(4)	0.22(10)	1.3(3)	2.26(9)	1.39(9)
HR 3282	78(6)	3.636(10)	3.28(8)	-3.45(20)	6.5(5)	1.47(8)	2.16(8)
HR 2411	22.7(10)	3.629(10)	2.18(6)	-0.72(14)	1.5(5)	1.90($\frac{16}{21}$)	1.73(19)
51 Hya	11.6(6)	3.629(10)	1.60(6)	0.74(16)	1.0(3)	2.30(12)	1.33(12)
RSG/AGB model	832	3.543	4.968	-7.68	12.0	-0.337	3.880
AGB model	429	3.405	3.841	-4.87	1.0	-0.830	4.235

^aRosseland radius in solar radius unit

^beffective temperature in K

^cempirical stellar luminosity in solar luminosity unit

^dbolometric magnitude

^estellar mass in solar mass unit

^fsurface gravity

^gpressure scaleheight in $\text{s}^2 \text{K cm}^{-1}$, from equation (2).

(depicted as a red open triangle in Fig. 6) mimics an RSG star, with $\mathcal{M} = 12 M_{\odot}$, $\mathcal{L} = 93\,000 L_{\odot}$, $T_{\text{eff}} = 3490 \text{ K}$, $\log g = -0.34$, and $\mathcal{R} = 832 R_{\odot}$ (Chiavassa et al. 2009, 2011b). The second (depicted as a red open circle in Fig. 6) is an AGB star simulation from Freytag & Höfner (2008), with $T_{\text{eff}} = 2542 \text{ K}$, $\log g = -0.83$, for a solar composition, with $\mathcal{M} = 1 M_{\odot}$, $\mathcal{L} = 6935 L_{\odot}$, and $\mathcal{R} = 429 R_{\odot}$. The final CSP values of these two simulations are computed in the following way:

(i) Using the radiative transfer code OPTIM3D (Chiavassa et al. 2009), we compute intensity maps from the 3D RHD simulations at the same wavelengths as those of the observation of the AGB-star W Ori. The simulation is scaled to approximatively match the angular diameter of W Ori (9.6 mas). For each wavelength, we adopt a top-hat filter with the same resolving power as the instrumental resolution ($\mathcal{R} = 1500$).

(ii) Using the method explained in Chiavassa et al. (2009), we calculate the Fourier transform of the intensity distributions, compute the triple product at the same interferometric baselines as for W Ori, and derive the final CSP value, as defined by equation (1).

The 3D RHD simulation predicts a CSP value of 11:9 for the AGB simulation ($\log \mathcal{H}_p = 4.235$), and of 3:4 for the RSG/AGB simulation ($\log \mathcal{H}_p = 3.88$). Two main physical sources drive the morphology of stellar surfaces, as predicted by RHD simulations:

(1) the dynamics (i.e. pulsation, rotation, convection, magnetism, etc.) is the first source of interferometric signal;

(2) and the temperature effect. The temperature inhomogeneities are caused by the convective movements, and for stars with T_{eff} lower than about 4000 K, the molecules are not dissociated and their contribution through the opacity in the photosphere is a second source of interferometric signal.

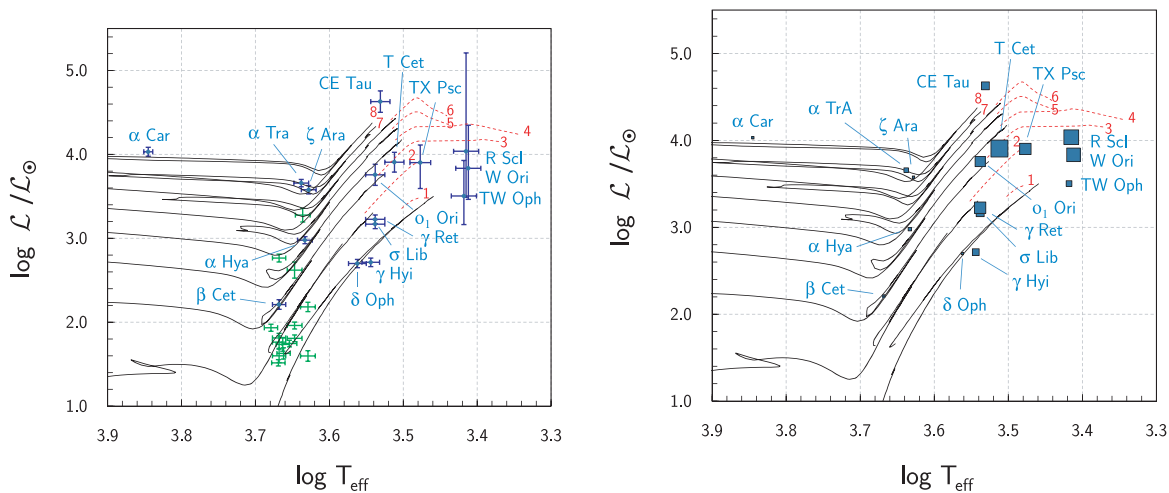


Figure 3. Temperature–luminosity diagrams for the targets of our sample, with evolutionary tracks (full lines, in black) and asymptotic giant branches (dashed lines, in red), for different masses (indicated at the end of each track, in red). Left-hand panel: error bars for the science targets (named, in blue) and the calibrators (unnamed, green crosses). Right-hand panel: CSP values for the science targets. For graphical convenience, the sizes of the (blue) squares are proportional to $\log(\text{CSP})$.

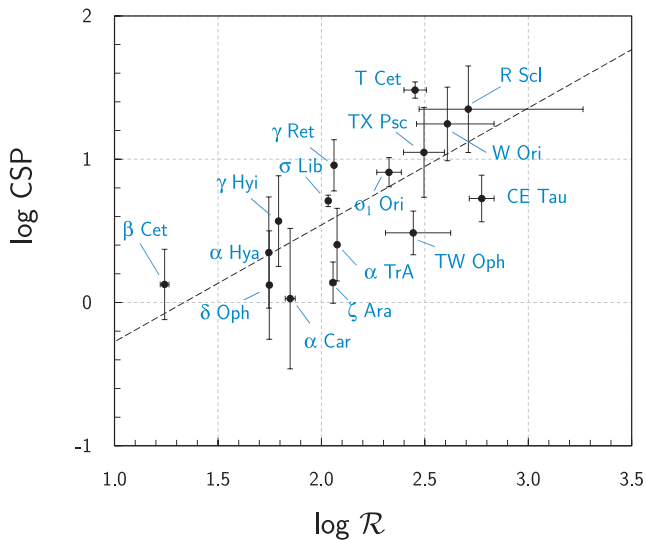


Figure 4. Asymmetry–radius diagram for the science targets. The equation of the dashed line (only drawn to fix the ideas; see text) is $y = 0.8152x - 1.0882$.

For stars with cool and diluted atmospheres (group II) like RSGs, the points (1), and (2) above contribute together to the stellar morphology. It is impossible to disentangle with CSP only what is contributing the most. Moreover, there is also a wavelength dependence of the contribution of (1) over (2), (1) prevailing at infrared wavelengths where we can see deeper in the photosphere, while (2) prevails in the visible where molecules show very large and deep electronic bands in their spectrum. Also for the AGBs, the situation is similar to RSGs but even more extreme (even larger CSP as we saw in the right-hand panel of Fig. 6), and finally there is also a difference between C-rich and O-rich stars. We believe this difference is due either to the molecules formed (point 2), or to the different model structure. In any case, O-rich stars should produce CSP values smaller than C-rich ones (see Section 2.3).

For stars with hot and compact atmospheres (group I), T_{eff} is larger than 4000 K (see Table 3). So there is ‘only’ the contribution

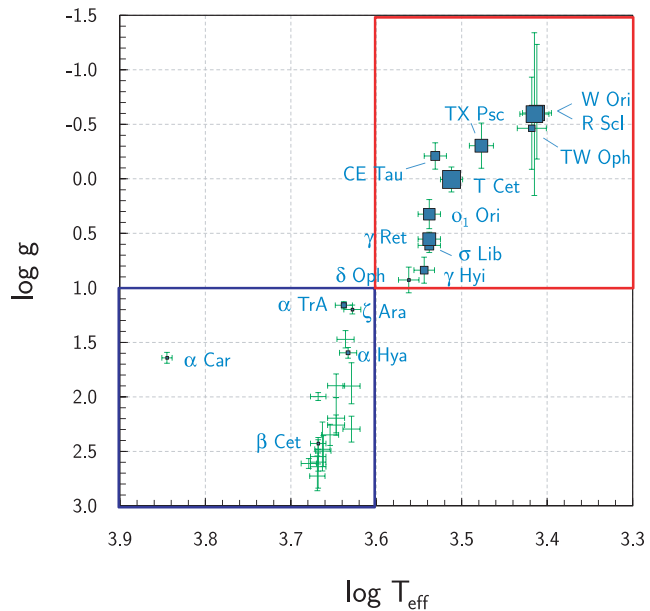


Figure 5. Temperature–gravity diagram, for the calibrators (unnamed, green crosses) and for the science targets (named, blue squares). The sizes of the squares are proportional to $\log(\text{CSP})$. Bottom-left box (blue): stars with hot and compact atmospheres (group I). Upper-right box (red): stars with cool and diluted atmospheres (group II).

of point (1) to the interferometric observables. So the CSP is lower than in the RSG/AGB case.

5 CONCLUSION

Using the CSP parameter derived from the measurements of the triple product integrated over the observation spectral band, we study the deviation from centrosymmetry of the brightness distribution for 16 well-resolved late-type stars. Observations took place on several runs distributed over a period of two years, using the ESO VLTI/AMBER facility in the K band at medium spectral resolution ($\mathcal{R} = 1500$).

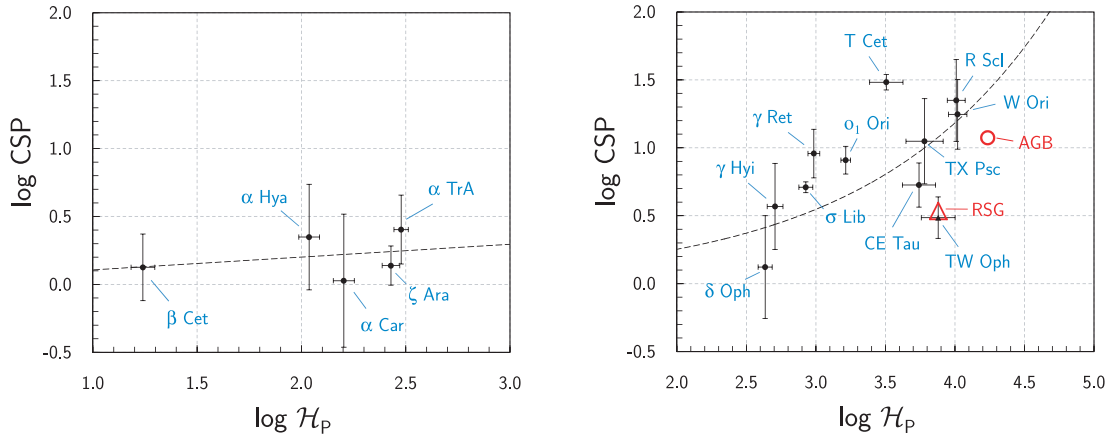


Figure 6. Asymmetry versus pressure scaleheight, for the science targets. Left-hand panel: stars with hot and compact atmospheres (group I). The equation of the dashed line is $y = 0.0942x + 0.0131$. Right-hand panel: stars with cool and diluted atmospheres (group II). The dashed curve is an exponential law with the following equation $y = 0.0541\exp(0.7714x)$ (see text for the choice of the laws). Open triangle (in red): RSG/AGB star simulation; open circle (red): AGB star simulation.

The values of CSP confirm that stars with the largest asymmetries are located in the upper right corner of the HRD. In separating hot and compact stellar atmospheres from cool and diluted atmospheres, we show that CSP increases with the atmospheric-pressure scaleheight \mathcal{H}_p , according to the following sequence: K giant, RSG, AGB. For the RSG and the AGB stars, this result is in agreement with the 3D RHD simulations.

ACKNOWLEDGEMENTS

The authors thank the ESO-Paranal VLTI team for supporting their AMBER observations, especially the night astronomers A. Mérand, G. Montagnier, F. Patru, J.-B. Le Bouquin, S. Rengaswamy, and W.J. de Wit, the VLTI group coordinator S. Brilliant, and the telescope and instrument operators A. and J. Cortes, A. Pino, C. Herrera, D. Castex, S. Cerda, and C. Cid. They also thank the Programme National de Physique Stellaire (PNPS) for supporting part of this collaborative research. AJ is grateful to B. Plez and T. Masseron for their ongoing support on the use of the MARCS code. CP is a PostDoc fellow supported by the Belgian Federal Science Policy Office via the PRODEX Programme of ESA. This study used the SIMBAD and VizieR data bases at the CDS, Strasbourg (France), and NASA ADS bibliographic services.

REFERENCES

Alvarez R., Plez B., 1998, *A&A*, 330, 1109
 Bertelli G., Girardi L., Marigo P., Nasi E., 2008, *A&A*, 484, 815
 Bertelli G., Nasi E., Girardi L., Marigo P., 2009, *A&A*, 508, 355
 Chiavassa A., Plez B., Josselin E., Freytag B., 2009, *A&A*, 506, 1351
 Chiavassa A. et al., 2010, *A&A*, 511, A51
 Chiavassa A. et al., 2011a, *A&A*, 528, A120
 Chiavassa A., Freytag B., Masseron T., Plez B., 2011b, *A&A*, 535, A22
 Cruzalèbes P., Spang A., Sacuto S., 2008, in Kaufer A., Kerber F., eds, Proc. 2007 ESO Instrument Calibration Workshop, Calibration of AMBER Visibilities at Low Spectral Resolution. Springer, Berlin, p. 479
 Cruzalèbes P., Jorissen A., Sacuto S., Bonneau D., 2010, *A&A*, 515, A6
 Cruzalèbes P. et al., 2013a, *MNRAS*, 432, 1658
 Cruzalèbes P. et al., 2013b, *MNRAS*, 434, 437
 Cruzalèbes P. et al., 2014, *MNRAS*, 443, 3550
 Efron B., Tibshirani R., 1993, *Monographs on Statistics and Applied Probability*, Vol. 57: An Introduction to the Bootstrap, edn. Chapman and Hall, London

Freytag B., 2001, in Garcia Lopez R. J., Rebolo R., Zapaterio Osorio M. R., eds, *ASP Conf. Ser. Vol. 223, 11th Cambridge Workshop on Cool Stars, Stellar Systems and the Sun*. Astron. Soc. Pac., San Francisco, p. 785
 Freytag B., Höfner S., 2008, *A&A*, 483, 571
 Freytag B., Steffen M., Ludwig H.-G., Wedemeyer-Böhm S., Schaffenberger W., Steiner O., 2012, *J. Comput. Phys.*, 231, 919
 Galassi M., Davies J., Theiler J., Gough B., Jungman G., Alken P., Booth M., Rossi F., 2009, *GNU Scientific Library Reference Manual*, 3rd edn. (v1.12). Network Theory (ISBN 0954612078)
 Gustafsson B., Edvardsson B., Eriksson K., Jørgensen U. G., Nordlund Å., Plez B., 2008, *A&A*, 486, 951
 Hofmann K., Balega Y., Scholz M., Weigelt G., 2000, *A&A*, 353, 1016
 JCGM-WG1, 2008, *Evaluation of Measurement Data - Guide to the Expression of Uncertainty in Measurement (JCGM 100:2008)*. BIPM, Paris
 Kervella P., Verhoelst T., Ridgway S. T., Perrin G., Lacour S., Cami J., Haubois X., 2009, *A&A*, 504, 115
 Mathur S. et al., 2011, *ApJ*, 741, L119
 Ohnaka K. et al., 2009, *A&A*, 503, 183
 Ohnaka K. et al., 2011, *A&A*, 529, A163
 Paladini C., Sacuto S., Klotz D., Ohnaka K., Wittkowski M., Nowotny W., Jorissen A., Hron J., 2012, *A&A*, 544, L5
 Plez B., 2012, *Astrophysics Source Code Library*, record ascl : 1205.004
 Ragland S. et al., 2006, *ApJ*, 652, L650
 Schwarzschild M., 1975, *ApJ*, 195, 137
 Svensson F., Ludwig H.-G., 2005, in Favata F., Hussain G. A. J., Battrick B., eds, *ESA SP-560: 13th Cambridge Workshop on Cool Stars, Stellar Systems and the Sun*. ESA, Noordwijk, p. 979
 Thompson R. R., Creech-Eakman M. J., Akeson R. L., 2002, *ApJ*, 570, L373
 Tuthill P. G., Haniff C. A., Baldwin J. E., 1997, *MNRAS*, 285, 529
 Tuthill P. G., Haniff C. A., Baldwin J. E., 1999, *MNRAS*, 306, 353
 van Belle G. T., Paladini C., Aringer B., Hron J., Ciardi D., 2013, *ApJ*, 775, 45
 Weiner J. et al., 2006, *ApJ*, 636, L1067
 Wilson R. W., Baldwin J. E., Buscher D. F., Warner P. J., 1992, *MNRAS*, 257, 369
 Wittkowski M. et al., 2011, *A&A*, 532, L7
 Wittkowski M., Hauschildt P. H., Arroyo-Torres B., Marcaide J. M., 2012, *A&A*, 540, L12
 Woodruff H. C., Tuthill P. G., Monnier J. D., Ireland M. J., Bedding T. R., Lacour S., Danchi W. C., Scholz M., 2008, *ApJ*, 673, L418

This paper has been typeset from a $\text{\TeX}/\text{\LaTeX}$ file prepared by the author.